J Mol Med (2013) 91:883–899
DOI 10.1007/s00109-013-0992-6

JMolMed

ORIGINAL ARTICLE

Stable tumor vessel normalization with pO_2 increase and endothelial PTEN activation by inositol trispyrophosphate brings novel tumor treatment

Claudine Kieda · Bouchra El Hafny-Rahbi · Guillaume Collet · Nathalie Lamerant-Fayel · Catherine Grillon · Alan Guichard · Jozef Dulak · Alicja Jozkowicz · Jerzy Kotlinowski · Konstantina C. Fylaktakidou · Aurélien Vidal · Philippe Auzeloux · Elisabeth Miot-Noirault · Jean-Claude Beloeil · Jean-Marie Lehn · Claude Nicolau

Received: 20 September 2012 / Revised: 24 December 2012 / Accepted: 2 January 2013 / Published online: 9 March 2013

Abstract Tumor hypoxia is a characteristic of cancer cell growth and invasion, promoting angiogenesis, which facilitates metastasis. Oxygen delivery remains impaired because tumor vessels are anarchic and leaky, contributing to tumor cell dissemination. Counteracting hypoxia by normalizing tumor vessels in order to improve drug and radio therapy efficacy and avoid cancer stem-like cell selection is a highly challenging issue. We show here that inositol trispyrophosphate (ITPP) treatment stably increases oxygen tension and blood flow in melanoma and breast cancer syngeneic models. It suppresses hypoxia-inducible factors (HIFs) and proangiogenic/glycolysis genes and proteins cascade. It selectively activates the tumor suppressor phosphatase and tensin homolog (PTEN) in vitro and in vivo at the endothelial cell (EC) level thus inhibiting PI3K and reducing tumor AKT phosphorylation. These mechanisms normalize tumor vessels by EC reorganization, maturation, pericytes attraction, and lowering progenitor cells recruitment in the tumor. It strongly reduces vascular leakage, tumor growth, drug resistance, and metastasis. ITPP

C. Kieda and B. El Hafny-Rahbi contributed equally to this study.

Electronic supplementary material The online version of this article (doi:10.1007/s00109-013-0992-6) contains supplementary material, which is available to authorized users.

C. Kieda (✉) · B. El Hafny-Rahbi · G. Collet · N. Lamerant-Fayel · C. Grillon · A. Guichard · J.-C. Beloeil
Centre de Biophysique Moléculaire, UPR CNRS 4301, rue Charles Sadron,
45071 Orléans Cedex 2, France
e-mail: claudine.kieda@cnrs-orleans.fr

J. Dulak · A. Jozkowicz · J. Kotlinowski
Department of Medical Biotechnology, Faculty of Biochemistry, Biophysics and Biotechnology, Jagiellonian University,
30-387 Kraków, Poland

K. C. Fylaktakidou · J.-M. Lehn · C. Nicolau
ISIS, Université de Strasbourg, 8 Allée Gaspard Monge,
67083 Strasbourg, France

J.-M. Lehn
e-mail: lehn@isis.u-strasbg.fr

C. Nicolau
e-mail: claude.nicolau@normoxys.com

A. Vidal · P. Auzeloux · E. Miot-Noirault
UMR 990 INSERM/Université d'Auvergne, "Imagerie moléculaire et thérapie vectorisée", 58, rue Montalembert,
63005 Clermont-Ferrand, France

C. Nicolau
NormOxys Inc., 300 Market Street,
Boston, MA 02135, USA

C. Nicolau
Friedman School of Nutrition Science and Policy, Tufts University,
Boston, MA 02115, USA

Present Address:
K. C. Fylaktakidou
Molecular Biology and Genetics Department, Democritus University of Thrace, Dimitras 19,
68100 Alexandropoulis, Greece

treatment avoids cancer stem-like cell selection, multidrug resistance (MDR) activation and efficiently enhances chemotherapeutic drugs activity. These data show that counteracting tumor hypoxia by stably restoring healthy vasculature is achieved by ITPP treatment, which opens new therapeutic options overcoming hypoxia-related limitations of antiangiogenesis-restricted therapies. By achieving long-term vessels normalization, ITPP should provide the adjuvant treatment required in order to overcome the subtle definition of therapeutic windows for in vivo treatments aimed by the current strategies against angiogenesis-dependent tumors.

Keywords Angiogenesis · Normalization · Oxygen · PTEN · Tumor hypoxia

Introduction

Tumor hypoxia, decisive for cancer progression, upregulates the hypoxia-inducible factors (HIFs), O_2 sensors in animal cells. Hypoxic tumor cells become resistant to radiotherapy and chemotherapy, getting to be highly aggressive and metastatic [1]. HIF-1α is associated with increased vessel numbers, tumor grade severity, poor prognostic, and treatment failure. Hypoxia-induced tumor angiogenesis [2] to build new vessels for oxygen and nutrients supply to tumor cells is in fact inefficient. It leads to incomplete vessels that are permeable and allow metastatic spreading of tumor cells escaping through nonsealed endothelial cells (ECs) [3]. Antiangiogenic strategies aiming at inhibition of tumor neo-vascularization have not provided lasting benefits because, by increasing tumor hypoxia, they result in selection of drug-resistant, aggressive cancer stem-like cells [4]. Tumor vessel normalization [5], rather than destruction, is a promising approach to cancer therapy since vessel abnormalization is now recognized as a hallmark of cancer [6]. The challenge is to counteract the vicious circle of hypoxia-induced abnormal vessels and tumor hypoxia maintained because of vessel defects [7].

New strategies aim at regulating intratumor vessels by reducing the activity of hypoxia sensors like PHD1-3 enzymes (prolyl hydroxylases), which target HIFs for degradation [8]. Vessel normalization beneficial effects were confirmed by the double antiangiogenic protein [9] targeting both vascular endothelial growth factor (VEGF) A [10] and angiopoietins, which restored tumor vessels efficacy. Vessel normalization prevents tumor cell dissemination [11], allows efficient delivery of cytotoxic drugs, and increases efficacy of radiotherapy [5] through control of HIFs activity [12].

Such approaches have allowed treatment protocols at time lapses defined as therapeutic windows during which vessels are normalized [13]. The technical difficulties to set adequate therapeutic windows prompted the search for long term normalization as an alternative goal for cancer antiangiogenesis therapy [14].

Hypoxia-induced angiogenesis is inhibited when human microvascular endothelial cells are cultured under hypoxic and flow conditions in the presence of RBCs loaded in vitro with ITPP [15] that overcame low oxygen tension (pO_2). In vitro, ITPP was shown to act as an allosteric effector of haemoglobin, and it was observed to reduce HIF-1α [16]. Given the central role that hypoxia plays in initiation and progression of neoplasms, these findings suggested a high potential for "oxygen tension compensation" in cancer therapy [15, 17] [18].

We tested here this hypothesis and the potential utility of ITPP to reach this challenge by treatment of melanoma and mammary cancer-bearing mice [19]. We show that ITPP treatment reduces tumor growth and eradicates lung metastasis. Biochemical changes in tumor and its microenvironment, upon ITPP treatment, appear to result predominantly, from the selective reversal of tumor hypoxia through vessel normalization. As an inositol phosphate derivative, ITPP molecule was tested for potential activation of endothelial phosphatase and tensin homolog (PTEN) and thus for its ability to bring a new tool to regulate angiogenesis independently of the cancer cell type. Indeed, drugs affecting the PTEN-regulated PI3K/AKT/mTOR pathway [20] that induces HIF-1α in a hypoxia-independent mechanism [21] may act on ECs to normalize tumor vessels. As PTEN is one of the most frequently mutated tumor suppressor, its inactivation leads to permanent AKT phosphorylation that maintains tumor growth. Consequently, this work was undertaken to check the hypothesis that ITPP treatment efficiently contributes to long-term vessel normalization through both oxygenation-dependent and oxygenation-independent control of HIF. We could show that angiogenesis regulation by ITPP treatment occurred through the downregulation of HIF-dependent proangiogenic genes. It regulated PTEN/AKT pathway by activating the endothelial PTEN that controls angiogenesis [22]. Resulting functional vessels were shown to facilitate access of chemotherapeutic agents to tumor cells. VEGF-induced leakiness was reduced, and invasive metastatic cell escape was abolished. Compensating intratumor hypoxia, treatment reduced the number of hypoxia- and multidrug-resistant as well as stemness-marker-positive tumor cells, reduced anaerobic glycolysis, and stopped the recruitment of HIF-mediated bone marrow derived $CXCR4^+$ precursor cells [23]. This work deciphers some aspects of the potent multifactorial therapeutic effects of ITPP treatment on neoplastic angiogenesis, inhibition of tumor growth, and prevention of metastasis through maturation of tumor vasculature and opens to new angiogenesis-based therapies of hypoxia-inducing diseases. It shows that ITPP provides means to reach the

goal of persistent angiogenesis normalization as an alternative to antiangiogenic therapies [14].

Materials and methods

Cells

Endothelial cells are FVB mouse lung microvascular endothelial cells (MLMEC FVB) [24, 25]. 4T1 murine breast cancer cells [19] were kindly provided by Professor Danuta Dus (IITD, PAN, Wroclaw, Poland). B16F10LucGFP are B16F10 murine melanoma cells, transduced with retroviral vectors containing a firefly luciferase complementary DNA (cDNA) driven by 5'LTR promoter followed by IRES sequence and enhanced green fluorescent protein cDNA (see Supplemental data). B16F10LucGFP cells were compared to B16F10 cells to validate their use in terms of similarity of growth and metastatic potential in vivo. Luciferase activity was shown not to be impaired by hypoxia, which could potentially affect the detection sensitivity (supplementary Fig. S1A).

Cell culture and oxygen regulation

The B16F10, B16F10LucGFP cell lines (see Supplemental data) and the 4T1 breast cancer cell line were cultured, respectively, in Dulbecco's modified Eagle medium and RPMI (Gibco) with 10 % fetal bovine serum (FBS) (PAA). The MLMEC-FVB endothelial cells were cultured in OptiMEM/2 % FBS. Cells were routinely cultured in a humidified incubator in 19.5 % oxygen and were oxygen-deprived in a Biotronix incubator allowing $p0_2$ regulation (1 %) and time setting.

Mouse subcutaneous melanoma and breast cancer models

C57BL6 mice and BALB/c mice were from Janvier Laboratory (France). Animal care and experimental procedures were approved by the CNREEA 03 Ethics Committee.

B16F10 or B16F10LucGFP cells were implanted in C57BL6 mice leg as subcutaneous tumors by injection of a plug constituted by 2×10^5 cells in 100 μl Matrigel™ (BD Biosciences) to help angiogenesis. 4T1 murine mammary carcinoma (10^4 cells in Matrigel) cells were injected in the mammary fat pad of BALB/c mice.

For the experimental metastases, see "Supplementary methods."

ITPP treatment and chemotherapeutic protocols

ITPP, prepared as described [16], was injected intraperitoneally (1.5 g/kg: in saline). Protocol consisting of serial treatments, over 4 weeks, was selected. It was started on day 7 and repeated on day 8 posttumor inoculation (day 0). The following serial treatments were applied on days 15 and 16, 21 and 22, and 28 and 29.

When combined with ITPP treatment, chemotherapeutic drugs, paclitaxel (2 mg/kg, in 50 % ethanol, 50 % chremophor EL; Calbiochem, per os) and cisplatine (*cis*-dichlorodiamine platinum) (10 mg/kg in saline; Sigma-Aldrich, intraperitoneally) were administered on days 9, 17, and 23, and the analyses were conducted on day 25.

Luciferase activity

Luciferase Assay System (Promega) was used as described by the manufacturer and luminescence quantified as relative light units per number of cells or per milligram of tissue with manual luminometer (Lumat LB9507).

Bioluminescence imaging was performed at the Center for Small Animal Imaging (TAAM, CNRS Orleans)

Cell staining for flow cytometry

Tumor cells were analyzed after tissue dissociation by collagenase/dispase (Gibco). For membrane antigen detection, single cell suspensions were incubated at 4 °C with respective primary antibodies for 1 h then with secondary antibodies for 30 min. For intracellular staining, cells were permeabilized by Cytofix/Cytoperm solution (BD Biosciences) as indicated, for 20 min before incubation with antibodies. Labeled primary antibodies used were the following: antimouse-CD31-PE (rat Ig-G2a, eBioscience) or CD31-PerCP (rat IgG2a, R&D), -VEGF R1-PE (Rat IgG2b, R&D), -VEGF R2-PE (Rat IgG2a, R&D), -CXCR4-PE (Rat IgG2b, R&D), -CD45-PerCP (rat IgG2b, R&D) or CD45-PE-Cy7 (rat IgG2b, R&D), -CD34-A700 (rat IgG2a, R&D). Unconjugated primary antibodies were the following: anti-Firefly Luciferase (Rabbit IgG, Abcam), anti-mouse -CD202 (Rat IgG1, eBiosciences), -HIF-2α (rabbit IgG, Abcam), -Lox (rabbit Ig-G, Novus Biologicals), -iNos (rabbit Ig-G, Transduction Laboratories), -Glut-1 (rabbit Ig-G, Santa-Cruz), -HO-1 (mouse Ig-G1, Abcam), -LDH (rabbit Ig-G, Santa-Cruz), -CAIX (rabbit Ig-G, Santa-Cruz), -CD133 (Rat IgG1, eBioscience), -Oct-3-4 (Rat IgG2a, R&D), or -ABCG2 (Rat IgG, Abcam). Binding was revealed by fluorescently-labeled anti-isotype secondary antibodies.

In specified experiments, tumors were depleted from $CD45^+$ and/ or $CD31^+$ cells by magnetic separation (Easy Sep magnet, StemCell Technologies Inc). Cytofluorimetry analyses were conducted on a FACS Sort (Becton Dickinson, Sunnyvale, CA, USA). Data were acquired on 5×10^4 to 10^5 cells and analyzed using CellQuest software (Becton Dickinson).

Immunohisto/cytological staining

Tumor tissues were embedded in tissue freezing medium (Tissue-Tek; Sakura) and snap frozen in liquid nitrogen. Tumor cryosections or cells were fixed and stained with mouse anti-CD31 (rat monoclonal IgG2a) (eBiosciences), anti-SMA (Rabbit IgG, Abcam), anti-P-glycoprotein (mouse IgG2a, Calbiochem), anti-CD133 (Rat IgG1, eBiosciences), anti-Phospho-AKT (Ser473) (Rabbit IgG), or anti-PTEN (rabbit IgG) (Cell Signalling) before tetramethyl rhodamine isothiocyanate or fluorescein isothiocyanate secondary antibodies were added. Nuclei were stained with bisbenzimide H 33258 (Sigma-Aldrich).

To assess hypoxic areas, pimonidazole (75 mg/kg, Hypoxyprobe™) was injected intravenously, 1 h before mice killing and tissue collection. Tumor cryosections were incubated with primary antipimonidazole antibodies (Mouse IgG1, Hypoxyprobe) before PE-labeled anti-mouse IgG antibodies were added.

PTEN localization and activation was studied on murine endothelial cells from lung (MLNEC FVB) that have been treated by hypoxia (22 h) and/or reoxygenation (25 h) in the presence or absence of ITPP (25 mM).

Fluorescent microscopy detection was performed on a Zeiss 200M inverted fluorescence microscope (Le Pecq, France), video microscopy station with controlled temperature, hygrometry, and gaz composition. Analysis was done with the Axiovision, software. Tumor necrosis was analyzed after hematoxylin–eosin staining of tumor sections.

Quantitative real-time PCR Total RNA was extracted from whole tumor using RNeasy Plus RNA extraction kit (Quiagen). cDNA was made with Transcriptor First strand cDNA Synthesis kit (Roche), and quantitative real-time PCR was performed with the QuantiTect SYBR Green RT-PCR kit (Qiagen), using LightCycler 480 (Roche). The data were analyzed with LightCycler 480 Software. Primers were supplied by Qiagen.

Magnetic resonance imaging

MR experiments on mice were performed on 9.4T horizontal magnet dedicated to small animal (94/21 USR Bruker Biospec, Wissembourg, France), equipped with a 950mT/m gradient set. Detailed method is given in "Supplementary methods." The animals were put under gaseous anesthesia during MRI exams (50 % N_2O, 0.7 l/min–50 % O_2, 0.7 l/min–Isoflurane, 1.5 %). Breathing rate was monitored by an air pillow placed on the mouse chest to adjust the anesthetic output. Magnetic resonance angiography-time of flight (MRA-TOF) experiment [26] allowed visualizing the 3D structure of the vascular tree of the tumor on the same animal. The total duration of the MRA experiment was 50 min. MRA sensitivity was increased by working at high field (9.4 T). Angiograms were produced using maximum intensity projections (MIPs) using Paravision 4.0 (Bruker). MRA-TOF is used for angiography, but this pulse sequence could also be seen as a "saturation recovery" pulse sequence (T1 sensitive). We have used it for detection of necrosis (Fig. 1b). Measurement of the tumor size was performed with a classical morphological spin-echo pulse sequence.

PO_2 and blood flow measurements

Mice were anesthetized by ketamine (Imalgène® 500, Rhone Mérieux, France) and xylazine (Rompun® 2 %, Bayer, France) (4:1 ratio) intraperitoneally injected (40 μl/20 g mouse) before the oxylite probe tips (Oxford optronics) were installed inside the tumor and oxygen pressure or blood flow recorded by the oxylite 2000E pO_2 or OxyFlow 2000 systems (Oxford Optronics) [27]. pO_2 was computed by determining the O_2-dependent fluorescence lifetime of ruthenium chloride on the tip of an optical fiber probe. The fluorescence lifetime is inversely proportional to the pO_2 in the tissue. The OxyFlow, a microvascular perfusion monitor, uses laser Doppler flowmetry established method for the measurement of blood perfusion with probe coupled to the O_2 probe tip.

[^{18}F]-FMISO PET imaging

For each animal anesthetized by ketamine/xylazine, [^{18}F]-FMISO PET imaging was performed using a device dedicated to small animal (eXplore VISTA®, GE Healthcare, USA). The spatial resolution of this system is given as 1.4 mm full width at half maximum at the center of the field of view [28].

Whole body images were acquired 1.30 h after i.v. administration of [^{18}F]-FMISO (8.9±1.3 MBq/mouse) for a total acquisition time of 20 min, an energy window set at 250–700 keV, two bed positions, and 6 ns coincidence-timing window. Image reconstruction used an ordered-subset expectation maximization (FORE/2D OSEM) method including corrections for radioactive decay, scanner dead time, and scattered radiation. No correction was applied for partial volume or attenuation.

Quantitative analysis of scans were performed using eXplore VISTA® workspace. Volume of interest (VOI) was delineated over tumor, and whole body, by summing multiple two-dimensional regions of interest from consecutive tomographic planes encompassing the entire uptake volume. The VOI of reference tissue was drawn on paw muscle and considered as background.

For each VOI, total activity was obtained as counts per minute (cpm), as well as mean activity in cpm per pixel and

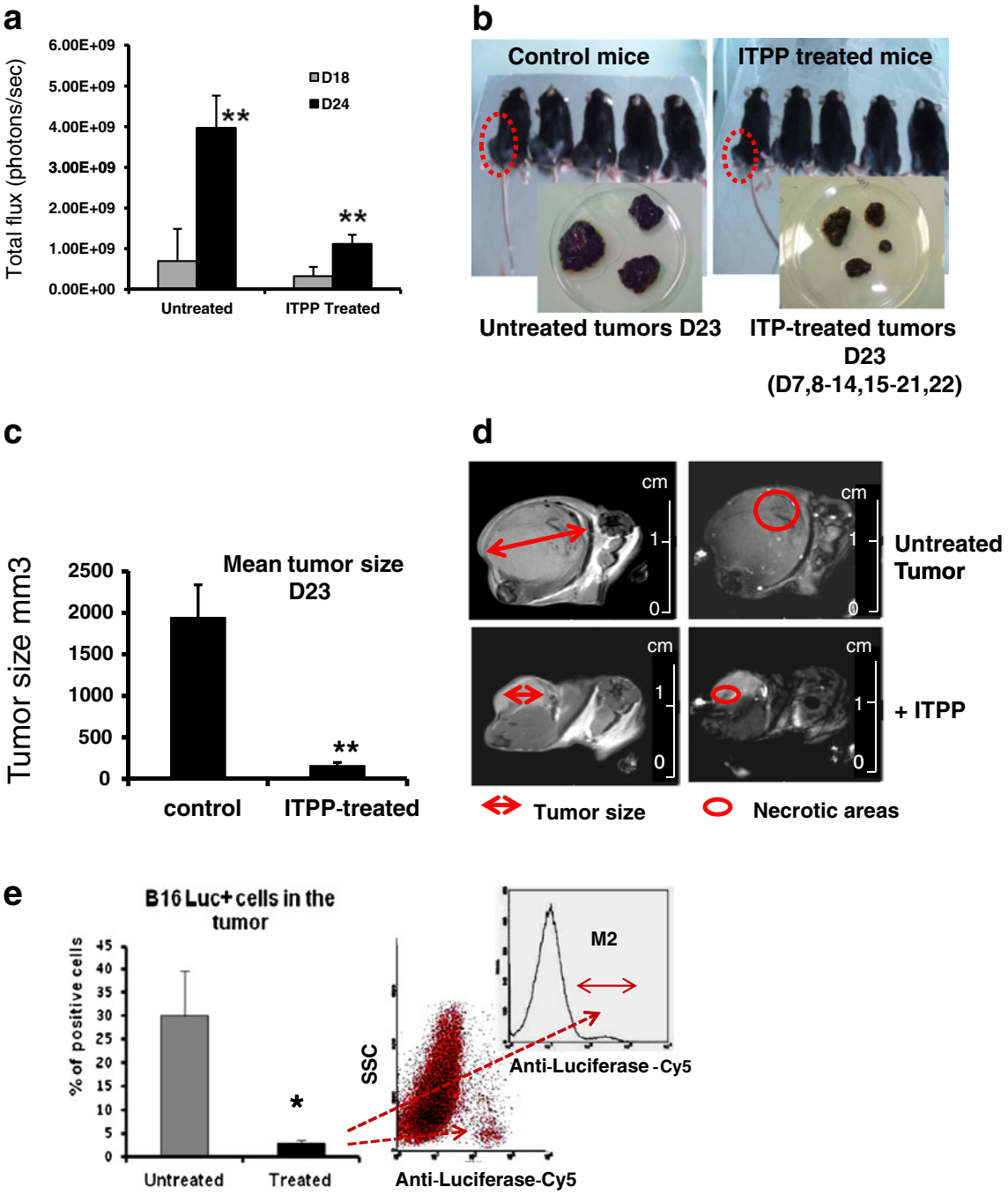

Fig. 1 ITPP reduces melanoma tumor growth and improves mice survival. **a** Effect of ITPP treatment on the kinetics of tumor growth measured by bioluminescence in treated and nontreated animals at days 18 and 24. Endpoint was fixed at 2 cm^3 ($n=6$ animals per group, one representative experiment out of $N>10$, $^{**}p<0.001$). **b** Comparison of tumor size, 23 days after B16F10LucGFP cells injection, showing reduced tumor growth in treated mice. Representative groups of five animals among groups of $n=10$ animals. One experiment out of $N\geq5$ separate experiments. *Insets* illustrate the extreme size ranges (minimal and maximal) that tumor reached in nontreated compared to treated mice. **c** Mean size of the tumors in treated and non treated animals at day 23 ($n=10$ in each group; number of experiments $N>20$, $^{**}p<0.001$). **d** Magnetic resonance imaging of B16 F10 induced tumor. Morphological pulse sequence (*left*). Strong volume variation of the tumor (untreated/ITPP=1163 mm^3/121 mm^3) was observed by image analysis after volume reconstruction. One typical example out of $n=10$/experimental group. MRA-TOF/saturation recovery pulse sequence (*right*): Necrotic areas appear darker. After ITPP treatment, their size decreased. One typical example out of $n=10$/experimental group. **e** Analysis by flow cytometry of B16LucGFP cells in tumors. Luciferase was detected intracellularly by specific antibodies and labeled by PerCP-Cy7 antirabbit IgG confirming: the reduced growth of tumor cells in ITPP-treated mice (%) and counts by direct cytometry analysis. Cells were numbered on the basis of intracellular Luciferase detection ($n=8$; $^{*}p<0.05$) from dot plots or inset from histogram analysis for quantification of B16F10LucGFP in the tumor

converted to cpm per milliliter using a calibration constant (obtained by imaging a mouse-size cylindrical calibration phantom containing a known activity of ^{18}F). By assuming a tissue density of 1 g/ml, VOI activity in cpm per milliliter was converted to cpm per gram. Tumor uptake was calculated by dividing total tumor activity (in cpm) by total whole body activity (in cpm).

Tumor capillary leakiness

It was assessed by Evans blue dye extravasion to the tumor interstitium. The dye was extracted by formamide [29]. The concentration measured spectrophotometrically was correlated to tumor weight.

Elisa detection of circulating VEGF

VEGF was assessed in serum (100 μl) by a typical sandwich ELISA kit for Mouse VEGF (Duo Set from R&D Systems). Assays were conducted according to the manufacturer's instructions.

Statistical analysis

Data represent mean±SD of 5 or 10 (when specified) representative experiments on $5 \leq n \leq 10$ animals in each group. Statistical significance was calculated by Student's t test ($p = 0.05$; $p = 0.001$; $n = 6$ animals per group, one representative experiment out of $N > 10$, $p < 0.001$).

Results

ITPP treatment counteracts melanoma tumor growth and lung metastases and improves mice survival

ITPP treatments produced a strong reduction of tumor growth assessed in terms of visible tumor size (Fig. 1b). The mean tumor weight at day 23 was 2.5±0.5 g and reduced to 0.5±0.2 g in treated animals ($n = 10$ per group and per experiment out of $N \geq 5$ separate experiments). This was precisely quantified by measurement of bioluminescence emission from B16F10Luc tumors measured at days 18 and 24, which increased 5.5-fold as compared to 2.8-fold in the treated animals, shown in Fig. 1a ($n = 6$ animals per group, one representative experiment out of $N > 10$, $p < 0.001$). Tumor growth reduction was quite visible in Fig. 1b showing the maximal and minimal sizes reached by tumors and the treatment effect, which is expressed as mean values of the tumor volumes at day 23 on Fig. 1c. MRI calculation of the tumor volume is precised on Fig. 1d. This was confirmed by the numbers of tumor cells detected in the tumor mass ranging from 30±7 % in nontreated animals, down to 3±1 % after ITPP treatment (Fig. 1e). Moreover, the metastatic invasion was drastically diminished. Indeed, in the subcutaneous model, no visible invasion but a faint Luciferase activity was detectable in lungs of treated animals (Fig. 2a). This difference was confirmed by artificial metastases assessment, after i.v. injection of B16F10LucGFP cells, which weakly developed in ITPP-treated animals compared to controls (Fig. 2b) ($n = 20$ in each group). These results corroborate the observed survival rate (Fig. 2d). Further on, no control animal was ethically allowed to survive longer than 30 days, as opposed to 100 % survival of ITPP-treated animals, which were killed on day 60 for further analyses. Endpoints were then fixed when tumors reached 2 cm^3. Indeed, Fig. 2c indicates that the total body weight of control animals clearly decreased compared to ITPP-treated tumor-bearing animals, despite the tumor growth. ITPP itself did not change the weight of the mice compared to saline injected mice, daily (Fig. 2c, inset).

ITPP treatment selectively counteracts hypoxia in the tumor microenvironment and normalizes tumor vessels

pO_2 was measured directly inside tumors before, during, and after ITPP treatment by intratumor assessment of the O_2-dependent fluorescence quenching of ruthenium. Nontreated tumors were strongly hypoxic ($pO_2 < 2$ mmHg). pO_2 measurement in real time inside the tumor showed that a first injection of ITPP caused a rapid pO_2 increase detectable after 30 min, reaching 40 mmHg within next 5 min (Fig. 3a). After serial injections of ITPP, as indicated in "Materials and methods," we show that the pO_2 level was stabilized at a high level for, at least, 72 h (Fig. 3b). Moreover, the pO_2 increase specifically concerned the hypoxic tumor site as, in the muscle of the contra lateral healthy leg of the same animal, no pO_2 change was detected by concomitant measurements (Fig. 3a). The validation of such hypoxia compensation by ITPP treatment was assessed and confirmed by performing the same experiments on murine breast cancer 4T1 model. Figure 3c gives typical data registered from one mouse out of 10 treated animals and showing a similar behaviour. A moderate increase was obtained after the first injection, and pO_2 strongly and stably increased after the second injection of ITPP. The reversal of intratumor hypoxia upon ITPP treatment was functionally paralleled by increased intratumor blood flow, measured concomitantly to pO_2, by laser Doppler and reported for day 22 tumors (Fig. 3d). Blood flow change may contribute to the rapid pO_2 increase and indicate a normalization of the tumor vessel function. Chemical confirmation of this process was assessed by histochemical detection of hypoxic sites in tumor. Hypoxic areas were evidenced by pimonidazole adducts formation with reduced proteins. Existing blood vessels, detected by double labeling for CD31

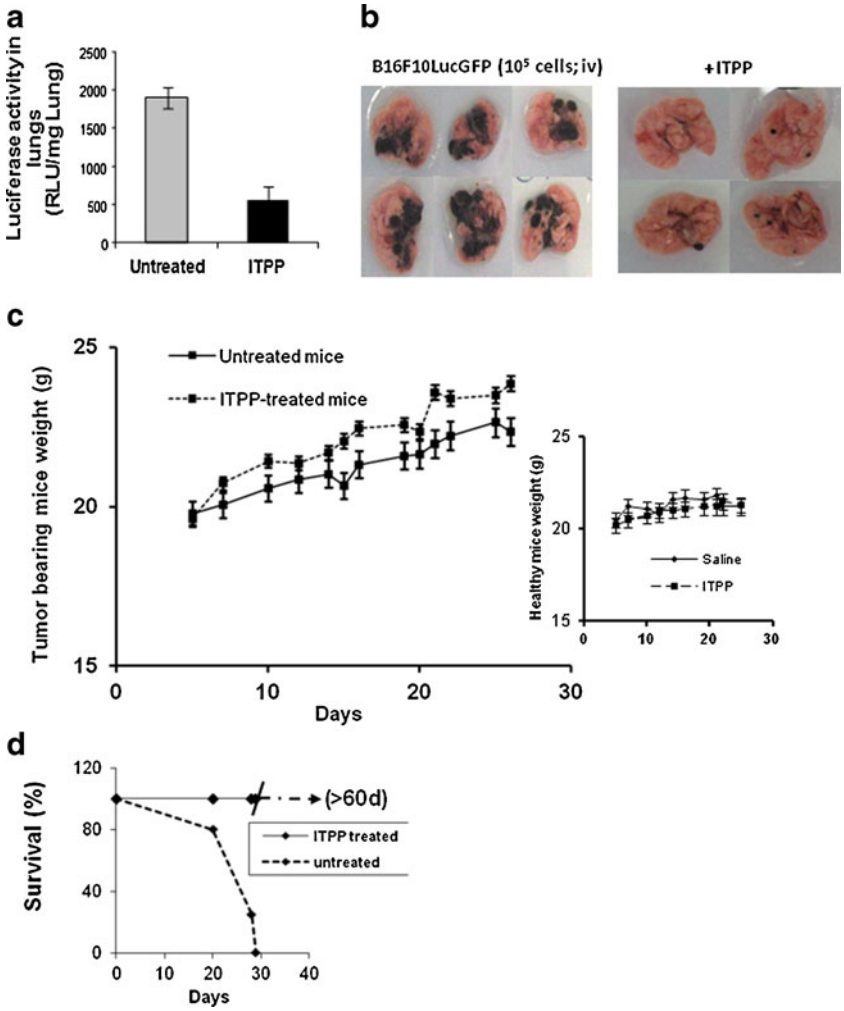

Fig. 2 Reduction of colonization and increased survival in cancer bearing mice treated by ITPP. **a** Reduced luciferase activity after ITPP treatment in lungs of mice bearing subcutaneously implanted melanoma, indicating reduced metastasis (n=8 ; p<0,001, one experiment out of 10). **b** Reduced lung colonization, after treatment, in artificial metastasis model where melanoma cells were injected intravenously. Representative samples out of 20 mice in each group. **c** Evolution of the animal body weights. Nontreated animals are losing weight compared to ITPP-treated animals (n=10 in each group, the number of experiments is N>10), *inset* shows the effect of daily ITPP injection compared to saline. **d** Survival curve showing the rescue of melanoma bearing mice treated by ITPP (n=10 in each group, one typical experiment out 5)

did not insure proper tissue oxygenation (Fig. 2e), confirming the poor efficacy of tumor angiogenesis. ITPP treatment prevented the formation of hypoxic areas, influencing deeply blood vessels structure, size, and density (Fig. 4a). These data were confirmed in living mice injected with [^{18}F]-FMISO to quantify hypoxia in the tumor (Fig. 4b). ITPP-treated mice clearly displayed restricted tumor growth and lower intratumor hypoxia. The tumor incorporation was expressed as Tact%=(total tumor activity/total whole body activity)×100. Upon ITPP treatment, Tact decreased from 14.58±0.52 % to 7.6±0.6 % (n=8 per group N=4).

ITPP treatment of tumor-bearing animals normalizes structure and function of vessels in the tumor

Vessel normalization was validated in live tumor-bearing animals upon ITPP treatment. Magnetic resonance imaging of tumor vasculature indicated strong structural changes. Typical chaotic tumor vessel architecture was observed by magnetic resonance angiography (MRA), while in ITPP-treated mice, vasculature appeared less dense but organized (Fig. 5a). Intratumor examination after treatment revealed CD31 labeling typical for endothelial cell, which delineates vessel-like structures after ITPP treatment as opposed to CD31$^+$ aggregates in controls (Fig. 5a). Furthermore, in treated tumors, vessel-like structures appear at the tumor periphery, surrounded by pericytes, positive for smooth muscle antigen (SMA$^+$) (Fig. 5a). Comparison with the dispersed SMA$^+$ labeled cells in the nontreated tumor mass suggests vessel normalization upon ITPP treatment. Confirmation of ITPP-induced vessel normalization is brought by pericytes recruited and lining the CD31$^+$ endothelial cells of the treated tumor vessels (Fig. 3a, d) as opposed to the random distribution of SMA$^+$ cells in nontreated tumor, shown by confocal microscopy (Fig. 5a). "Normalization" accompanied a strong reduction of tumor size (Figs. 1 and 5a).

Normalization was confirmed in terms of vessel function, first by reduction of tumor vessels permeability. Evans blue leakage was significantly diminished after two sequential treatments by ITPP (Fig. 5b) correlating with the reduced concentration of circulating VEGF, the main vessel

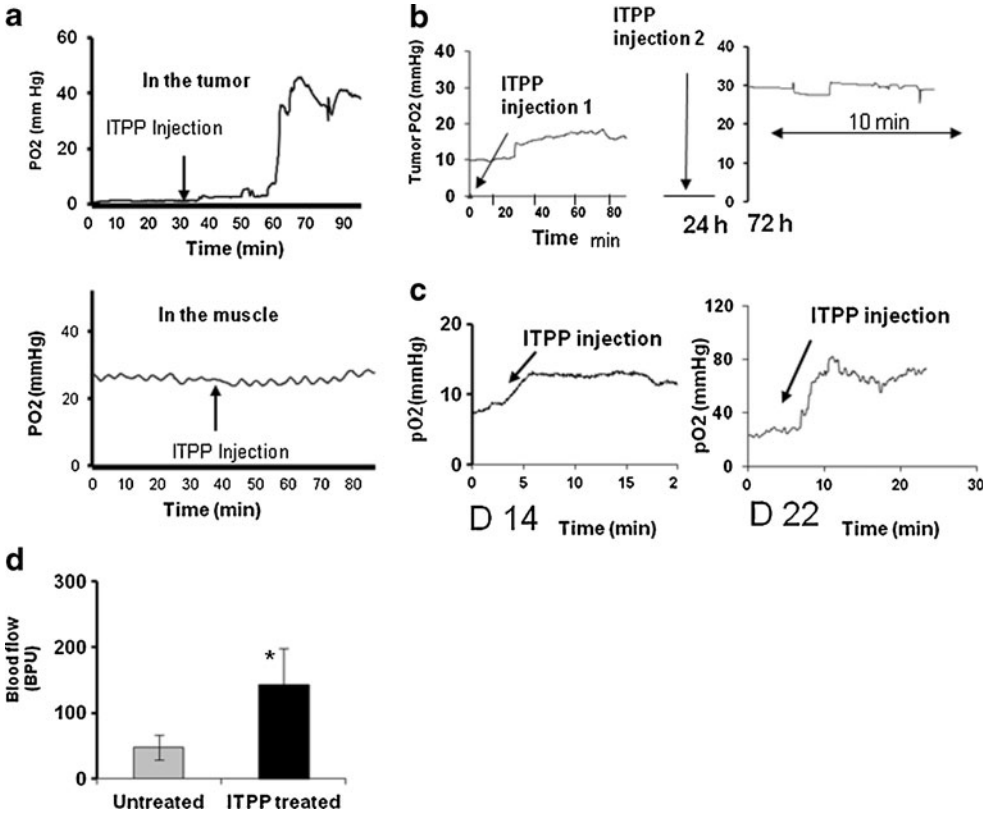

Fig. 3 Improved tumor oxygenation in cancer bearing mice treated by ITPP. **a** ITPP treatment increases oxygen pressure specifically inside a melanoma tumor within 30 min. No pO_2 modification was observed in the healthy muscle. The probe was maintained in the same place, and pO_2 was recorded in real time. Figure reports a representative example out of five animals treated the same day; identical data were acquired from $n>50$ mice treated by ITPP. **b** Tumor oxygen pressure increase after double injection of ITPP is stable up to 72 h. Tumor oxygen pressure is enhanced 30 min after the first injection of ITPP. A second injection of ITPP applied after 24 h increases and stabilizes the pO_2 increase for at least 72 h. Figure reports typical measurements randomly performed in treated animals ($n=10$ per experiment). **c** ITPP treatment increases oxygen pressure inside a 4T1 breast tumor within 10 min. The increased pO_2 (12 mmHg at day 14) is stable over 1 week (20 mmHg at day 22) and enhanced once more after a second ITPP injection. Picture shows data typically reporting several measurements randomly performed in treated animals ($n=8$ per experiment). **d** Laser Doppler signals showing tumor blood flow improvement in ITPP-treated mice. Measurements were done randomly in each tumor treated as described in "Materials and methods," day 22 ($n=8$ out of 10 per group; $p<0.05$)

permeant growth factor (Fig. 5c). ITPP-induced vessel maturation was shown by reduction of the invasive index [30]. $CD105^+/CD31^+$ ratio measures endoglin (CD105) versus PECAM-1 (CD31) expressing endothelial cells and reflects tumor neo-angiogenic activity. $CD105^+/CD31^+$ cells ratio, calculated among tumor $CD45^-$ cells, was lowered upon ITPP action (Fig. 5d), mainly because $CD31^+$ cell number increased (Fig. 5a, d). The strong enhancement of VEGF receptors 1 and 2 on nonleukocyte $CD31^+$ $CD45^-$ cells upon treatment (Fig. 5e) confirms maturation of blood vessels reflecting direct interactions of endothelial cells with mural pericytes (Fig. 5a).

$CD31^+$ cell numbers increased among the whole tumor population (Fig. 5f) and was accompanied by enhancement of the hypoxia-dependent, endothelial tyrosine kinase Tie-2 receptor for angiopoietins 1 and 2 (Fig. 5f and Supplementary Fig. 2d), a marker of matured vessels [6, 10].

ITPP treatment induces tumor vessels maturation by regulating hypoxia-sensitive molecules

Hypoxia-sensitive genes turning on tumor angiogenesis displayed drastic changes upon ITPP treatment of tumor-bearing animals. Since the ITPP effect was associated with pO_2 changes in the tumor, the levels of HIF-1 and HIF-2, crucial for cell response to oxygen, were analyzed by quantitative PCR. Figure 6a shows the strong downregulation of messenger RNA (mRNAs) for $HIF1^-$ and HIF2, corroborating the reduction of HIF1 and HIF2 protein expression (Supplementary Fig. S2 and Fig. 6a, respectively) and indicating that regulation occurred at the transcriptional level. HIFs mRNA and O_2-dependent molecules like VHL and the tumor protective and proangiogenic enzyme HO-1 mRNAs were considerably reduced by ITPP (Fig 6a). Main oxygen sensors in angiogenesis, PHD-1, PHD-2, and PHD-3, are

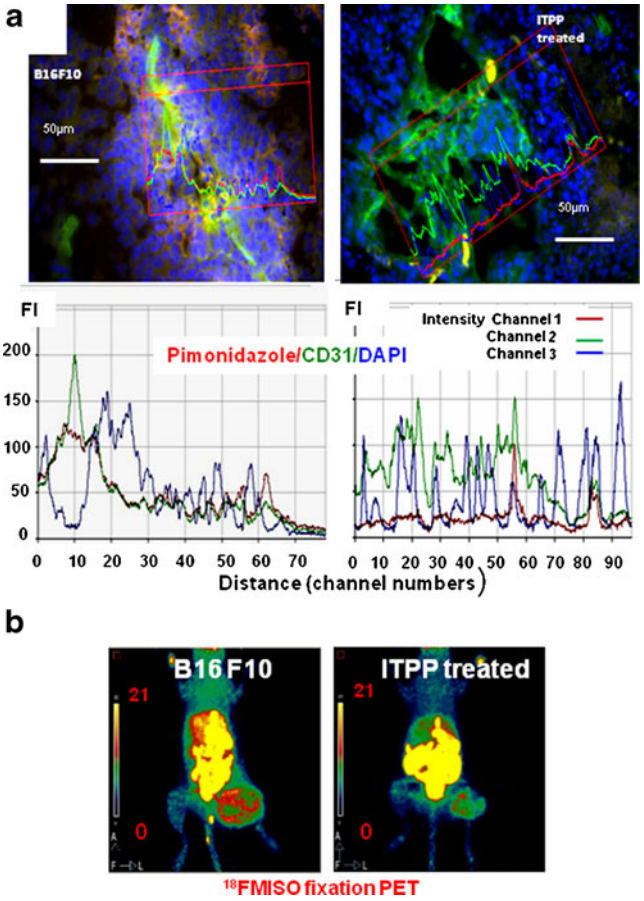

Fig. 4 Reduction of hypoxia in cancer bearing mice treated by ITPP. **a** Images showing CD31$^+$ blood vessels (*green*) and hypoxic sites detected by pimonidazole staining (*red*), in tumor sections. Nuclei are in *blue*. Pimonidazole was i.p. injected, 1 h before killing then staining by anti pimonidazole antibodies. After ITPP treatment, no staining for hypoxia was visible in tumors and weakly detected by image analysis estimating the fluorescence intensities and distribution in the green and red channels. One representative picture out $N>10$ experiments ($n=10$ animals per group). **b** Quantification by PET imaging of hypoxia by [^{18}F]-FMISO fixation in melanoma bearing mice 14 days after subcutaneous implantation of the tumor cells (*left*, control) and upon serial ITPP treatments (*right*). The tumor radioactivity incorporation was quantified and expressed as: % of tumor activity=(total tumor activity/total whole body activity)×100. After ITPP treatment, the tumor activity decreased from 14.58±0.52 % (controls) to 7.6±0.6 % ($n=8$ animals in each group) showing the reversal of tumor hypoxia ($N=4$). Representative PET imaging of control and treated animals, normalized with the same color scaling (0–21 on both images)

considerably underexpressed in treated animals, indicating a direct regulation by pO_2, as described for VHL mRNA induction by hypoxia.

Increase in CD31, VEGFR1, and VEGFR2 mRNAs (Fig. 6a) confirmed the enhancement of corresponding protein-expressing cell numbers and the maturation effect observed among CD45$^-$ cells (Fig. 5d) with the general increase in Tie2$^+$ cell numbers (Fig.5e). mRNA for osteopontin, a key molecule of the tumor stroma, decisive for tumor invasion and known to be regulated by the PTEN/AKT pathway in melanoma, was strikingly reduced by ITPP treatment (Fig. 6a).

In accordance with the finding that ITPP treatment did not influence endothelial cells growth in vitro [15] but controlled the angiogenic process, its in vivo effect might implicate activation of PTEN that controls both hypoxia-dependent and hypoxia-independent mechanisms of tumor angiogenesis. We observed a clear reduction of the SDF1/CXCR4-dependent recruitment of endothelial precursor cells from the bone marrow. They cooperate to tumor angiogenesis by integrating neovessels in a PTEN/PI3-K/AKT/eNOS dependent process. Figure 6b shows the drastic reduction of the proportion of CXCR4$^+$, CD34$^+$, and CD45$^-$ endothelial precursors cells, recruited inside the tumor upon ITPP treatment.

ITPP-induced tumor vessel normalization regulates energetic metabolism molecules linked to oxidative stress

The number of cells expressing stress- and metastasis-related markers not only HIF2 but also lysyl oxydase (LOX) was assessed. Hypoxia-regulated LOX, involved in invasiveness [31] and responsible for H_2O_2 production that inactivates PTEN [32], was drastically reduced by ITPP in the whole tumor (Fig. 6c).

Moreover, upon ITPP treatment, LOX and HIFs were both efficiently downregulated in their mRNA expression (Supplementary Fig. S2). In parallel, the endothelium-restricted enzyme, inducible NO synthase, produces NO that induces vessel dilatation and VEGF production responsible for permeabilization. Here, the number of cells expressing INOS [33] was significantly reduced (Fig. 6c), similarly to HO-1. The artificial metastasis model confirmed the beneficial effects of ITPP treatment (Supplementary Fig. S2).

Tumor cells resist to poor oxygen supply using the anaerobic glycolysis as source of energy. This rescue pathway starts with enhanced Glut-1 receptor expression ending with lactate release, activating glycolytic pathway enzymes, such as lactate dehydrogenase (LDH) [34] and carbonic anhydrase IX (CAIX), a key enzyme allowing tumor cell survival in hypoxia and acidic pH [35]. Numbers of cells expressing Glut-1 receptors, LDH and CAIX, were drastically reduced upon ITPP treatment (Fig. 6d), indicating a significant reversal of hypoxia-induced resistance.

ITPP-treatment-induced tumor vessel maturation involves activation of endothelial PTEN

As the above data point to PTEN-mediated controls of angiogenesis upon ITPP treatment, PTEN activation was first studied in situ. In tumors, endothelial cells displayed a

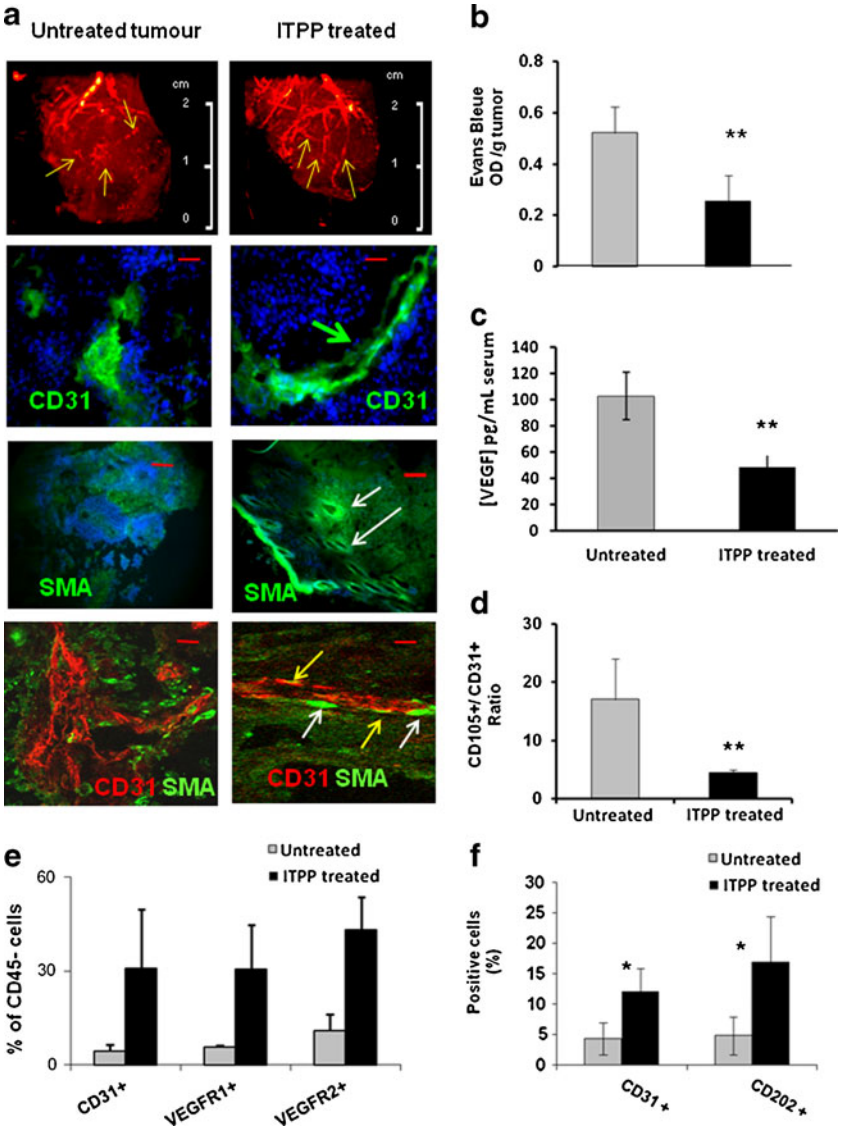

Fig. 5 Morphological and functional tumor vessel normalization induced by ITPP treatment. **a** ITPP-induced vessel normalization in ITPP-treated mice compared to untreated tumors imaged by: magnetic resonance angiography, 20 days after tumor induction showing chaotic vessel architecture in nontreated tumor (*left panel*, *yellow arrows*), vessel reorganization (normalization, *yellow arrows*, *right panel*) in ITPP-treated melanoma-bearing mice accompanied by tumor size reduction (see scale). Representative images from a typical example among 10 separate experiments. CD31 immunostaining of vascular endothelial cells in tumor sections showing disorganized aggregates in non treated tumors ($n=10$) and vessel-like structures (*green arrow*) in treated mice ($n=10$). Nuclei are stained with DAPI (*blue*); immunohistochemical staining for smooth muscle actin (SMA^+) pericytes (*white arrows*) in frozen sections showing vessel organization in tumors from ITPP-treated mice (*right panel*, $n=10$) compared to non-treated animals (*left panel*, $n=10$). Tumor vessel architecture observed by confocal microscopy (Zeiss, LSM) imaging showing the close proximity of smooth muscle actin (SMA)-stained pericytes (*green*) with $CD31^+$ endothelial cells (*red*) in the organized and normalized vessels, after ITPP treatment ($n=10$) compared to nontreated tumor-bearing mice ($n=10$). Scale bars represent 50 μm. **b** Reduction of tumor vessel leakiness measured by permeability to Evans Blue diffusion in tumor ($n=8$; $*p=0{,}001$). **c** Assessment of circulating VEGF by ELISA ($n=8$; *, $p=0{,}001$). **d** Angiogenesis-associated Endoglin (CD105) related to CD31 endothelial cell marker, quantified by flow cytometry among CD45-depleted tumor population, predicting endothelial cells lower activity and motility after treatment ($n=8$; $**p=0.001$). **e** Increased $CD31^+$ and $VEGF\text{-}Rs^+$ cells, in CD45 depleted tumor population after ITPP treatment ($n=10$/group; $*p=0.05$). **f** Flow cytometry analysis showing endothelial cells maturation markers: enhanced CD31 and Tie-2 (CD202) expressing cell numbers ($n=10$/group; $*p=0.05$)

clear redistribution of PTEN getting distinct from CD31 labeling (Fig. 7a) while they colocalized before treatment (Fig. 7a). Concomitantly, a strong general decrease in AKT phosphorylation (Fig. 7b) in endothelial cells and the tumor tissue confirmed PTEN control of angiogenesis [22] and the efficient reversal of tumor hypoxia (Fig. 4a).

As PTEN activity requires its relocation from the cytoplasm towards the membrane [36], we attempted to decipher

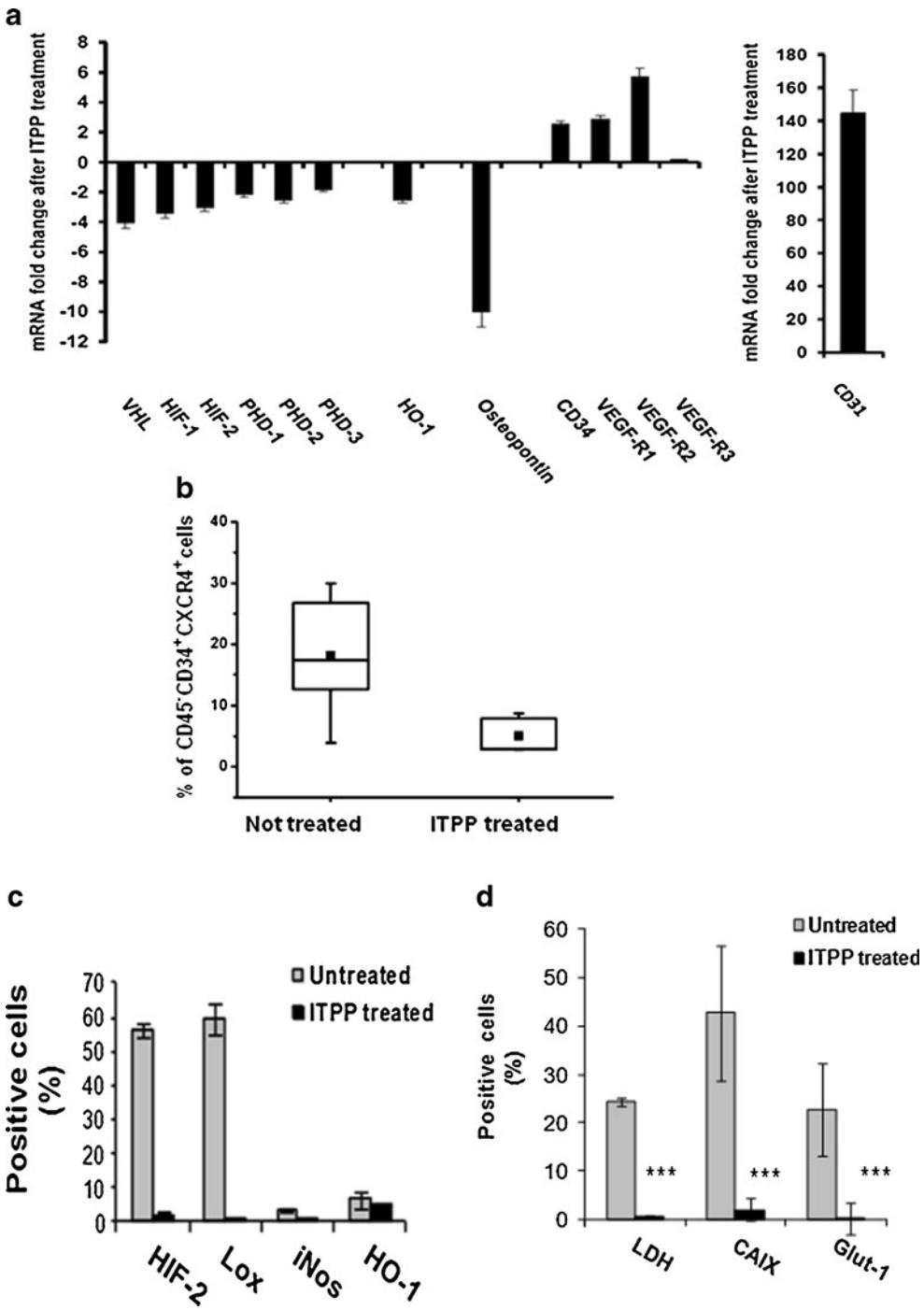

Fig. 6 Phenotypic effect of ITPP treatment on tumor metabolism. **a** RT-PCR analysis revealing: downregulation of hypoxia/oxygen sensing genes and prometastasis genes; upregulation of genes implicated in endothelial cells maturation. Results are percent of non treated samples level (n=8 animals, five separate experiments; **p=0.001; ***p=0.0001). **b** Reduction of the number of $CXCR4^+$ $CD34^+$ $CD45^-$ precursor cells among tumor cells upon ITPP treatment. Quantification by flow cytometry from separate tumor samples (n=10/group $p<0.001$). **c** Flow cytometry quantitative analysis showing a dramatic decrease in the number of cells expressing hypoxia-, stress-, and metastasis- related markers in primary tumors (day22) after ITPP treatments as described in "Materials and methods" (n=8/group; 5 separate experiments, **p=0.001; ***p=0.0001). **d** Flow cytometry quantification analysis showing a dramatic decrease in the number of cells expressing markers of high energetic metabolism in primary tumors (day22) after ITPP treatments as described in "Materials and methods" (n=8/group; five separate experiments; ***p=0.0001)

in vitro the direct effect of ITPP on PTEN activation in endothelial cells, by hypoxia/reoxygenation experiments conducted in the presence and/or absence of ITPP. Organo-specific murine lung endothelial cells showed a reorganisation of PTEN in the presence of ITPP (Fig. 8). PTEN first detected in the whole cytoplasm, colocalizing mainly with CD31 (Fig. 8a) migrated upon treatment with ITPP, towards the plasma membrane more efficiently in hypoxia (Figs. 5 and 7b) than in normoxia (Fig. 8a). This effect of ITPP was clearly enhanced in experiments involving hypoxia/reoxygenation (Fig. 8c) performed to mimic the in vivo sequence of events that occur during angiogenesis as shown by the preferential relocation in elongated endothelial cells (Fig. 8c insets).

ITPP-induced tumor vessels normalization prevents resistant cancer stem-like cells formation

In the ITPP-treated animals, reduction of p-glycoprotein expression among cells in the tumor (Fig. 9a) suggests that

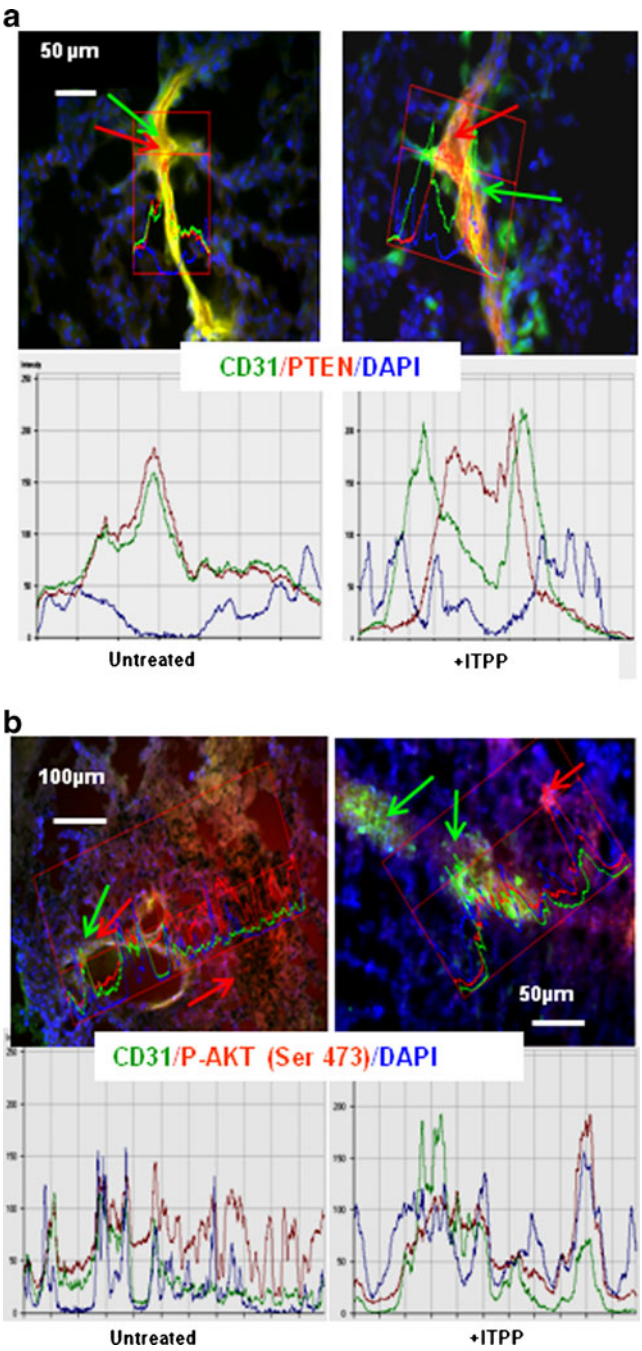

Fig. 7 Effect of ITPP treatment on activation of endothelial PTEN and loss of tumor AKT phosphorylation. **a** PTEN, P-AKT (Ser473) and CD31 immunostainings. PTEN was expressed (*red arrows*) and colocalized with $CD31^+$ endothelial cells (*green arrows* and *green*/*red* channels analysis of the label distribution, by image analysis) in non-treated tumor-bearing animals (*left panel*, $n=10$/group). Markers separately localized after ITPP treatment (*right panel*, $n=10$/group). The *red*/*green* channels display separate distribution by image analysis. **b** P-AKT distribution over the tumor (*red arrows* and *red curve* of the image analysis) observed in tumor stroma and endothelial cells, colocalized with CD31 staining (*green arrows* and *green curve*) in non-treated tumors. Expression of P-AKT was strongly reduced to punctual sites upon ITPP treatment. Image analysis point the separate localization with CD31 (*right four panels*, $n=10$/group)

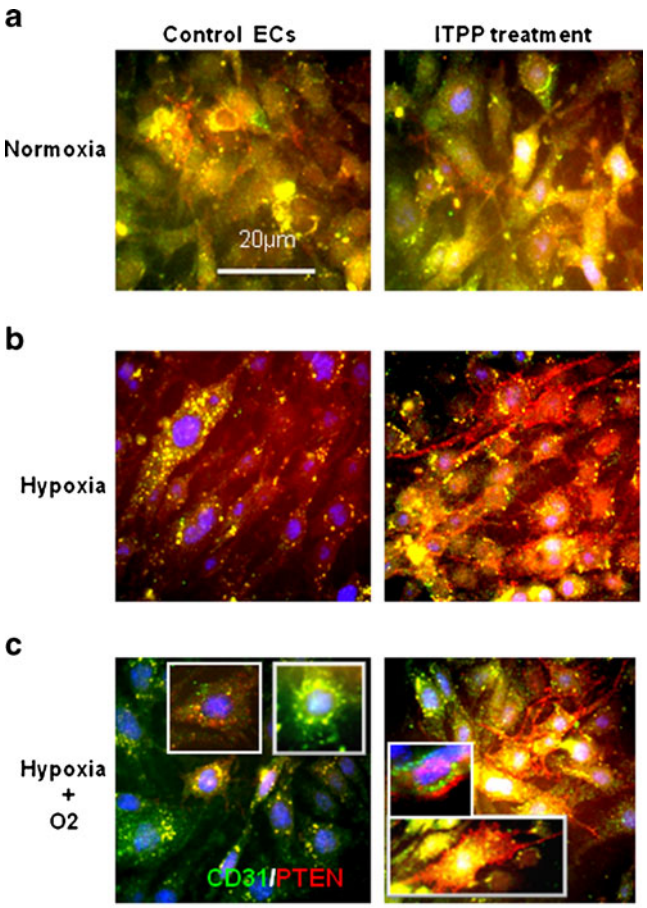

Fig. 8 Effect of ITPP on activation of endothelial PTEN in vitro upon hypoxia reoxygenation. In vitro activation of endothelial PTEN by ITPP upon hypoxia reoxygenation experiments. Murine lungs endothelial cells, MLuMEC cell line immortalized from FVB mice, were submitted to hypoxia (25 h) (**b**) then reoxygenated (22 h) (**c**) in the presence or not of ITPP (25 mM). PTEN activation was evidenced by its relocalization from the cytoplasm in hypoxia towards the inner face of the plasma membrane upon ITPP treatment. ITPP induced localization effect of PTEN was as enhanced by reoxygenation

hypoxia-induced loss of sensitivity to drugs, due to multidrug efflux pumps (MDRs), could be reversed by tumor reoxygenation. This is confirmed by the reduction upon ITPP treatment of the number of cells positive for ABCG-2 [35], which is a drug exclusion pump typical for stem cells, as well as other stemness markers, i.e., CD133 and Oct 3–4 that were detected in highly positive tumor cell subpopulations before treatment (Fig. 9b).

ITPP-induced tumor vessels normalization favors chemotherapy

As ITPP treatment improves O_2 delivery to hypoxic tissues and normalizes vessels, we studied its effect on melanoma treatment by drugs such as paclitaxel and cisplatin. Combined ITPP and drug treatments acted positively and led to

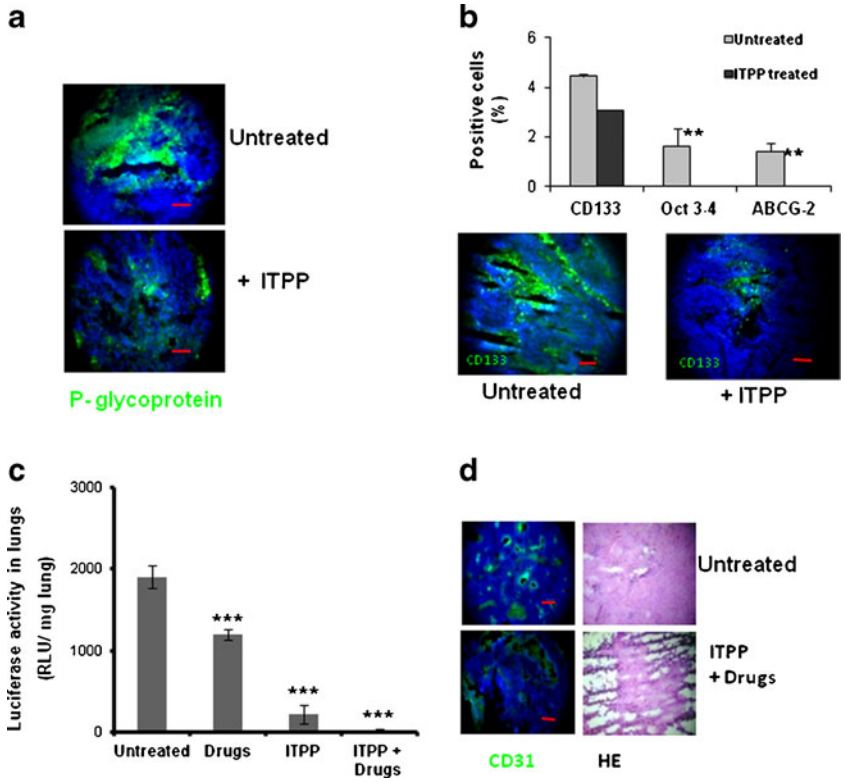

Fig. 9 Effect of ITPP treatment on tumor hypoxia-induced resistance, stem cell selection, and enhancement of chemotherapeutic efficacy. **a** The P-glycoprotein immunostaining showing a reduced number of multidrug resistance positive tumor cells after ITPP treatment. Frozen sections of primary tumors from experiments described in Fig. 6 were histochemically labeled (day22, ITPP treatments as described in "Materials and methods" (n=8/group; five separate experiments). Scale bars=50 μm. **b** Quantification by flow cytometry showing the reduction of cells positive for precursor and stem cell-associated markers (CD133, Oct3-4, ABCG-2) after ITPP treatment. $CD133^+$ immunostaining corroborated the reduction visible on frozen section staining of primary tumors as in **a**. Scale bars=50 μm. **c** Lung metastasis is suppressed by chemotherapeutic drugs (Paclitaxel and Cisplatin), when treatment is preceded by ITPP injection. Tumor cells are detected by their Lucifease activity in the lungs of animals from control, ITPP, CisPt plus Paclitaxel and combined treatments $ITPP^+$ drugs as described in "Materials and methods." Data are reported for day22 (n=10/group; 5 experiments; ***; p=0.001). **d** CD31 staining of endothelial cells (*green*) and eosin/hematoxylin staining obtained in primary tumor frozen sections from experiment described in **c**. Efficient tissue necrosis was obtained when chemotherapeutic treatment is preceded by ITPP injection as described in "Materials and methods." Scale bars=50 μm

eradication of metastatic tumor cells from lungs as shown for day22 in Fig. 9c. The $CD31^+$ microvessels density was reduced when animals were treated by ITPP/drugs as compared to numerous and poorly structured microvessels, $CD31^+$ endothelial cells in controls (Fig. 8d). pO_2 and vessel normalization preceding drug treatment favored drugs cytoxicity, as indicated by necrotic areas corresponding to diffuse CD31 positivity and delineated by H&E staining (Fig. 9d). These data stress the potential of ITPP in combined therapies.

Discussion

When pO_2 in tumor microenvironment is brought to normal levels, tumor cells do not invade surrounding tissues and do not metastasize. This work shows that this effect is due to normalization of tumor angiogenesis into matured vessels resulting from selective compensation of hypoxia and control of PTEN/AKT pathway through endothelial cell membrane PTEN activation by ITPP treatment.

Intratumor neo-vessel strengthening may explain the reduction of metastatic cells escape from primary tumors. ITPP treatment indeed resulted in vessels normalization, through endothelial cells acquisition of a matured phenotype and reorganization of the vessel tumor microenvironment. Here, vessels strengthening, shown by pericyte alignment and maturation was confirmed by the induction of VEGF receptors in response to the pericyte/EC cross-talk [37]. Moreover, Tie-2, a specific endothelial tyrosine kinase receptor reduced in hypoxia and essential for normal blood vessel maturation by attracting pericytes upon binding of angiopoietin-1, was increased, corroborating the ITPP effect on vessel maturation. This was confirmed by the reduced invasive index reporting that the tumor angiogenic activity [30] through CD31-positive endothelial cell increases, while

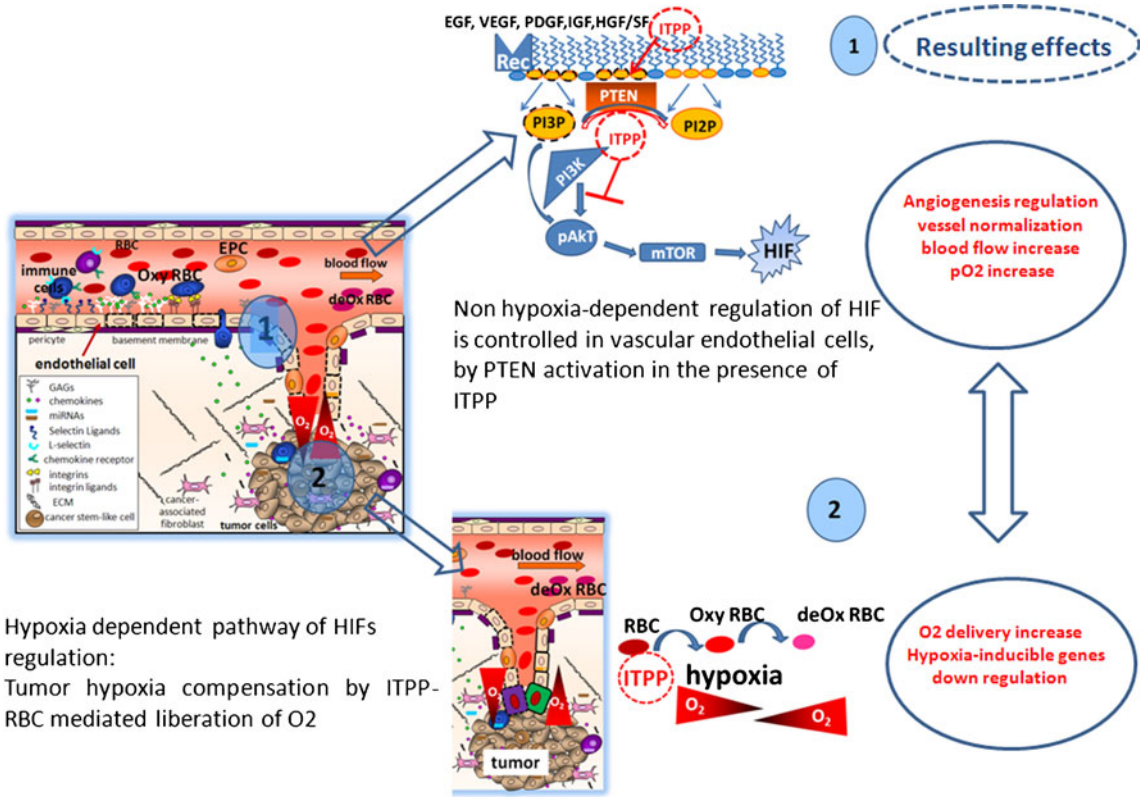

Fig. 10 Schematic outline of the proposed action of ITPP on HIFs regulation. *1* ITPP regulates angiogenesis by activating PTEN that inhibits PI3K action, AkT phosphorylation and mTOR actitivy towards HIF at the endothelial cell level. This regulates the vessels and increases the blood flow, while *2* hypoxia mediated O_2 delivery by ITPP, allosteric effector of hemoglobin [15–18], increases the intra tumor pO_2, which also acts to destabilize HIF1α and down regulates VEGFs and VEGFs-related gene cascade. This directly reduces the endothelial cell mobilization, activation and growth, thus regulating the tumor VEGF-mediated pathological angiogenesis

CD31, ensuring endothelial cell junction and vessel efficacy, is reduced by hypoxia [38]. ITPP-treatment effect on the number and function of $CD31^+$ cells confirms vessel normalization and differs deeply from $CD31^+$ cell reduction, which results from antiangiogenic treatments.

The O_2-dependent HIFs pathway is regulated by ITPP treatment. PHD/HIF regulatory axis is described as a promising therapeutic target to disable tumor capacity to adjust to hypoxia and control cell survival. Inhibition of residual PHDs shown here would avoid feedback protection of HIF and reduce tumor resistance to hypoxia [39].

Moreover, similarly to HIF-1α mRNA [40], other O_2-dependent mRNAs like VHL mRNA, regulated by the O_2-sensitive angiomiR 92-1 [41] and the tumor protective and proangiogenic enzyme HO-1 [42], were considerably reduced by ITPP treatment. Our data on PHDs and VHL mRNA reduction in long-term-treated tumors might reflect the whole tumor stroma response to stable reoxygenation and to reduced level of HIFs mRNAs, downregulating their regulatory proteins mRNA as described [43].

Vessel strengthening control of tumor cell escape is accompanied by a remarkable reduction of mRNA for osteopontin. Disappearance of such key molecule of tumor stroma helps explain the reduction of tumor cell dissemination. Osteopontin is indeed decisive for tumor invasion [44] and known to be regulated by the PTEN/AKT pathway in melanoma [45]. This strong modification of the tumor stroma reaction upon ITPP treatment was linked to the PTEN activation at the endothelial cell level, thus independent of the PTEN status of the tumor cells.

Contributing to control cell dissemination, activation of PTEN is favored here by downregulation of LOX expression. Indeed, local production of H_2O_2 by LOX would inactivate the tumor suppressor—PTEN—explaining the positive regulation loop between LOX and HIF in cancer development [32]. As PTEN activation was shown at the endothelial cell level, it implies that ITPP treatment has for main target the vascular cell biology. It restores the PTEN-mediated control on tumor angiogenesis due to activated AKT through the PDK/PI3K/AKT/mTOR pathway [22]. Effect on endothelial cells was indeed associated with a strong general decrease in AKT phosphorylation in the tumor mass confirming PTEN control of normal vs pathological angiogenesis and the efficient reversal of tumor hypoxia [46].

ITPP treatment is clearly targeting the vasculature. It is thus applicable to angiogenesis-dependent pathologies independently of the PTEN tumor suppressor mutations that occur in the majority of tumors.

The biological significance of the above described effect on PTEN activation is further illustrated by its effect on the recruitment of endothelial precursors, the second main mechanism by which tumors build angiogenesis [47]. Among the bone marrow derived cells that are recruited by the tumor to help its progression, endothelial precursors are mobilized to integrate tumor forming neovessels mainly by the SDF1/CXCR4 axis. This work shows the drastic reduction of the proportion of $CXCR4^{+}$, $CD34^{+}$, $CD45^{-}$ cells, and endothelial precursors recruited in response to tumor SDF-1 chemoattraction, which is PTEN/AKT dependent [48].

Consequently, ITPP treatment contributes to restore vessel wall integrity and efficient blood supply by counteracting both hypoxia-dependent and hypoxia-independent HIF induction as summarized on Fig. 10. ITPP action appears to contribute in control of both mechanisms. The part played by PTEN vs O_2 delivery could not be directly shown using endothelial cell-specific mutation of Pten (Tie2CrePten) in mice. Tie2CrePtenflox/+ mice only being viable [22]. Such normalization is known to result in improved chemotherapeutics delivery by efficient and, as shown here, nonpermeable mature vessels. It also reverted stem-like resistant invasive phenotype of tumor cells, prevented activation of glycolysis pathway shown by the numbers of cells expressing Glut-1 receptors, LDH and CAIX, which were drastically reduced upon ITPP treatment. Indicating an efficient reversal of hypoxia-induced resistance towards drug and cancer stem-like cells selection ITPP treatment contributed to the efficiency of chemotherapy [33].

Indeed, ITPP-induced vessel normalization was accompanied by the reduction of drug efflux pumps thus counteracting chemo-resistance built by MDRs [34]. It also reduced drastically the number of cancer stem cells as opposed to their selection operated by the strong intratumor hypoxia, which results from antiangiogenic therapies using monoclonal antibodies—bevacuzimab (Avastin) against VEGF-A or VEGFR2 inhibitors (Sunitinib) as documented [4, 49]. Our data help to explain why antiangiogenic cancer therapies provide poor results and why drug-induced improvement of vascular health correlates with better cancer prognosis. This work shows the strength of such an approach allowing stable vessel normalization. This important effect of ITPP should overcome the problem of adequate therapeutic windows for future therapies.

Our data stress the potential of ITPP in combined therapies. ITPP should provide the adjuvant needed to chemo- and radiotherapy efficacy providing enhanced O_2 supply and vessel normalization [5, 12], an alternative to antiangiogenic strategies [14].

Collectively, these findings highlight the multifactor and potent therapeutic use of ITPP and demonstrate its fundamental interest for advancing therapy of hypoxia and angiogenesis-dependent pathologies.

Acknowledgments Thanks are due to Dr. Michael Morin (OncoVax, Boston, MA, USA) and to Dr Agata Matejuk (Le_Studium, senior research fellow) for reading the manuscript. The authors thank David Gosset, Michèle Mitterrand, and Frédéric Szeremeta, for their skillful technical help in flow cytometry, biological and MRI experiments, respectively; Emilie Cardamone is thanked for technical help for in vivo imaging acquisition.

Grant support/disclosure This work was partly supported by the grant no. 347/N-INCA/2008/0 from the Polish Ministry of Science and Higher Education and CNRS and by the French National Research Agency (ANR 3Sens). AJ is a recipient of the Wellcome Trust Senior Research Fellowship in Basic Biomedical Science. This work was financed by Normoxys Inc. under contract, within the research agreement between the Company and the University of Strasbourg.
Claude Nicolau is shareholder in NormOxys Inc.

References

1. Semenza GL (2004) Intratumoral hypoxia, radiation resistance, and HIF-1. Cancer Cell 5:405–406
2. Folkman J (2007) Angiogenesis: an organizing principle for drug discovery? Nat Rev Drug Discov 6:273–286
3. Carmeliet P (2003) Angiogenesis in health and disease. Nat Med 9:653–660
4. Paez-Ribes M, Allen E, Hudock J, Takeda T, Okuyama H, Vinals F, Inoue M, Bergers G, Hanahan D, Casanovas O (2009) Antiangiogenic therapy elicits malignant progression of tumors to increased local invasion and distant metastasis. Cancer Cell 15:220–231
5. Jain RK (2005) Normalization of tumor vasculature: an emerging concept in antiangiogenic therapy. Science 307:58–62
6. Goel S, Duda DG, Xu L, Munn LL, Boucher Y, Fukumura D, Jain RK (2011) Normalization of the vasculature for treatment of cancer and other diseases. Physiol Rev 91:1071–1121
7. Carmeliet P, Jain RK (2011) Principles and mechanisms of vessel normalization for cancer and other angiogenic diseases. Nat Rev Drug Discov 10:417–427
8. Kaelin WG Jr, Ratcliffe PJ (2008) Oxygen sensing by metazoans: the central role of the HIF hydroxylase pathway. Mol Cell 30:393–402
9. Koh YJ, Kim HZ, Hwang SI, Lee JE, Oh N, Jung K, Kim M, Kim KE, Kim H, Lim NK et al (2010) Double antiangiogenic protein, DAAP, targeting VEGF-A and angiopoietins in tumor angiogenesis, metastasis, and vascular leakage. Cancer Cell 18:171–184
10. Yancopoulos GD, Davis S, Gale NW, Rudge JS, Wiegand SJ, Holash J (2000) Vascular-specific growth factors and blood vessel formation. Nature 407:242–248
11. Mazzone M, Dettori D, Leite de Oliveira R, Loges S, Schmidt T, Jonckx B, Tian YM, Lanahan AA, Pollard P, Ruiz de Almodovar C et al (2009) Heterozygous deficiency of PHD2 restores tumor

oxygenation and inhibits metastasis via endothelial normalization. Cell 136:839–851
12. Semenza GL (2012) Hypoxia-inducible factors: mediators of cancer progression and targets for cancer therapy. Trends Pharmacol Sci 33:207–214
13. Carmeliet P, Jain RK (2011) Molecular mechanisms and clinical applications of angiogenesis. Nature 473:298–307
14. Sato Y (2011) Persistent vascular normalization as an alternative goal of anti-angiogenic cancer therapy. Cancer Sci 102:1253–1256
15. Kieda C, Greferath R, Crola da Silva C, Fylaktakidou KC, Lehn JM, Nicolau C (2006) Suppression of hypoxia-induced HIF-1alpha and of angiogenesis in endothelial cells by myo-inositol trispyrophosphate-treated erythrocytes. Proc Natl Acad Sci U S A 103:15576–15581
16. Fylaktakidou KC, Lehn JM, Greferath R, Nicolau C (2005) Inositol tripyrophosphate: a new membrane permeant allosteric effector of haemoglobin. Bioorg Med Chem Lett 15:1605–1608
17. Sihn G, Walter T, Klein JC, Queguiner I, Iwao H, Nicolau C, Lehn JM, Corvol P, Gasc JM (2007) Anti-angiogenic properties of myo-inositol trispyrophosphate in ovo and growth reduction of implanted glioma. FEBS Lett 581:962–966
18. Aprahamian M, Bour G, Akladios CY, Fylaktakidou K, Greferath R, Soler L, Marescaux J, Egly JM, Lehn JM, Nicolau C (2011) Myo-inositoltrispyrophosphate treatment leads to HIF-1alpha suppression and eradication of early hepatoma tumors in rats. ChemBioChem 12:777–783
19. Chen L, Huang TG, Meseck M, Mandeli J, Fallon J, Woo SL (2007) Rejection of metastatic 4 T1 breast cancer by attenuation of Treg cells in combination with immune stimulation. Mol Ther 15:2194–2202
20. Qayum N, Muschel RJ, Im JH, Balathasan L, Koch CJ, Patel S, McKenna WG, Bernhard EJ (2009) Tumor vascular changes mediated by inhibition of oncogenic signaling. Cancer Res 69:6347–6354
21. Harada H, Itasaka S, Kizaka-Kondoh S, Shibuya K, Morinibu A, Shinomiya K, Hiraoka M (2009) The Akt/mTOR pathway assures the synthesis of HIF-1alpha protein in a glucose- and reoxygenation-dependent manner in irradiated tumors. J Biol Chem 284:5332–5342
22. Hamada K, Sasaki T, Koni PA, Natsui M, Kishimoto H, Sasaki J, Yajima N, Horie Y, Hasegawa G, Naito M et al (2005) The PTEN/PI3K pathway governs normal vascular development and tumor angiogenesis. Genes Dev 19:2054–2065
23. Du R, Lu KV, Petritsch C, Liu P, Ganss R, Passegue E, Song H, Vandenberg S, Johnson RS, Werb Z et al (2008) HIF1alpha induces the recruitment of bone marrow-derived vascular modulatory cells to regulate tumor angiogenesis and invasion. Cancer Cell 13:206–220
24. Bizouarne N, Denis V, Legrand A, Monsigny M, Kieda C (1993) A SV-40 immortalized murine endothelial cell line from peripheral lymph node high endothelium expresses a new alpha-L-fucose binding protein. Biol Cell 79:209–218
25. Denis V, Dupuis P, Bizouarne N, de O Sampaio S, Hong L, Lebret M, Monsigny M, Nakache M, Kieda C (1996) Selective induction of peripheral and mucosal endothelial cell addressins with peripheral lymph nodes and Peyer's patch cell-conditioned media. J Leukoc Biol 60:744–752
26. Fauconnier M, Bourigault ML, Meme S, Szeremeta F, Palomo J, Danneels A, Charron S, Fick L, Jacobs M, Beloeil JC et al (2011) Protein kinase C-theta is required for development of experimental cerebral malaria. Am J Pathol 178:212–221
27. Elas M, Ahn KH, Parasca A, Barth ED, Lee D, Haney C, Halpern HJ (2006) Electron paramagnetic resonance oxygen images correlate spatially and quantitatively with oxylite oxygen measurements. Clin Cancer Res 12:4209–4217
28. Wang Y, Seidel J, Tsui BM, Vaquero JJ, Pomper MG (2006) Performance evaluation of the GE healthcare eXplore VISTA dual-ring small-animal PET scanner. J Nucl Med 47:1891–1900
29. Dolinay T, Wu W, Kaminski N, Ifedigbo E, Kaynar AM, Szilasi M, Watkins SC, Ryter SW, Hoetzel A, Choi AM (2008) Mitogen-activated protein kinases regulate susceptibility to ventilator-induced lung injury. PLoS One 3:e1601
30. Tachezy M, Reichelt U, Melenberg T, Gebauer F, Izbicki JR, Kaifi JT (2010) Angiogenesis index CD105 (Endoglin)/CD31 (PECAM-1) as a predictive factor for invasion and proliferation in intraductal papillary mucinous neoplasm (IPMN) of the pancreas. Histol Histopathol 25:1239–1246
31. Erler JT, Bennewith KL, Nicolau M, Dornhofer N, Kong C, Le QT, Chi JT, Jeffrey SS, Giaccia AJ (2006) Lysyl oxidase is essential for hypoxia-induced metastasis. Nature 440:1222–1226
32. Sonveaux P, Vegran F, Schroeder T, Wergin MC, Verrax J, Rabbani ZN, De Saedeleer CJ, Kennedy KM, Diepart C, Jordan BF et al (2008) Targeting lactate-fueled respiration selectively kills hypoxic tumor cells in mice. J Clin Invest 118:3930–3942
33. Airley RE, Loncaster J, Raleigh JA, Harris AL, Davidson SE, Hunter RD, West CM, Stratford IJ (2003) GLUT-1 and CAIX as intrinsic markers of hypoxia in carcinoma of the cervix: relationship to pimonidazole binding. Int J Cancer 104:85–91
34. Song X, Liu X, Chi W, Liu Y, Wei L, Wang X, Yu J (2006) Hypoxia-induced resistance to cisplatin and doxorubicin in non-small cell lung cancer is inhibited by silencing of HIF-1alpha gene. Cancer Chemother Pharmacol 58:776–784
35. Monzani E, Facchetti F, Galmozzi E, Corsini E, Benetti A, Cavazzin C, Gritti A, Piccinini A, Porro D, Santinami M et al (2007) Melanoma contains CD133 and ABCG2 positive cells with enhanced tumourigenic potential. Eur J Cancer 43:935–946
36. Vazquez F, Matsuoka S, Sellers WR, Yanagida T, Ueda M, Devreotes PN (2006) Tumor suppressor PTEN acts through dynamic interaction with the plasma membrane. Proc Natl Acad Sci U S A 103:3633–3638
37. Lorquet S, Berndt S, Blacher S, Gengoux E, Peulen O, Maquoi E, Noel A, Foidart JM, Munaut C, Pequeux C (2010) Soluble forms of VEGF receptor-1 and −2 promote vascular maturation via mural cell recruitment. FASEB J 24:3782–3795
38. Carreau A, Kieda C, Grillon C (2011) Nitric oxide modulates the expression of endothelial cell adhesion molecules involved in angiogenesis and leukocyte recruitment. Exp Cell Res 317:29–41
39. Henze AT, Riedel J, Diem T, Wenner J, Flamme I, Pouyseggur J, Plate KH, Acker T (2010) Prolyl hydroxylases 2 and 3 act in gliomas as protective negative feedback regulators of hypoxia-inducible factors. Cancer Res 70:357–366
40. Galban S, Gorospe M (2009) Factors interacting with HIF-1alpha mRNA: novel therapeutic targets. Curr Pharm Des 15:3853–3860
41. Ghosh AK, Shanafelt TD, Cimmino A, Taccioli C, Volinia S, Liu CG, Calin GA, Croce CM, Chan DA, Giaccia AJ et al (2009) Aberrant regulation of pVHL levels by microRNA promotes the HIF/VEGF axis in CLL B cells. Blood 113:5568–5574
42. Was H, Cichon T, Smolarczyk R, Rudnicka D, Stopa M, Chevalier C, Leger JJ, Lackowska B, Grochot A, Bojkowska K et al (2006) Overexpression of heme oxygenase-1 in murine melanoma: increased proliferation and viability of tumor cells, decreased survival of mice. Am J Pathol 169:2181–2198
43. Turcotte S, Desrosiers RR, Beliveau R (2004) Hypoxia upregulates von Hippel-Lindau tumor-suppressor protein through RhoA-dependent activity in renal cell carcinoma. Am J Physiol Renal Physiol 286:F338–F348
44. Shevde LA, Das S, Clark DW, Samant RS (2010) Osteopontin: an effector and an effect of tumor metastasis. Curr Mol Med 10:71–81

45. Packer L, Pavey S, Parker A, Stark M, Johansson P, Clarke B, Pollock P, Ringner M, Hayward N (2006) Osteopontin is a downstream effector of the PI3-kinase pathway in melanomas that is inversely correlated with functional PTEN. Carcinogenesis 27:1778–1786
46. Obara D, Utsugisawa K, Nagane Y, Tohgi H (2002) Hypoxic condition interferes with phosphorylation of Akt at Thr(308) in cultured rat pheochromocytoma-12 cells. Neurosci Lett 332:167–170
47. Chouaib S, Kieda C, Benlalam H, Noman MZ, Mami-Chouaib F, Ruegg C (2010) Endothelial cells as key determinants of the tumor microenvironment: interaction with tumor cells, extracellular matrix and immune killer cells. Crit Rev Immunol 30:529–545
48. Zheng H, Fu G, Dai T, Huang H (2007) Migration of endothelial progenitor cells mediated by stromal cell-derived factor-1alpha/CXCR4 via PI3K/Akt/eNOS signal transduction pathway. J Cardiovasc Pharmacol 50:274–280
49. Ebos JM, Lee CR, Cruz-Munoz W, Bjarnason GA, Christensen JG, Kerbel RS (2009) Accelerated metastasis after short-term treatment with a potent inhibitor of tumor angiogenesis. Cancer Cell 15:232–239